Inorganic Chemistry

pubs.acs.org/IC Article

Photoactivated Osmium Arene Anticancer Complexes

Xuling Xue, Ying Fu, Liang He, Luca Salassa, Ling-Feng He, Yuan-Yuan Hao, Madeleine J. Koh, Clément Soulié, Russell J. Needham, Abraha Habtemariam, Claudio Garino, Kirill A. Lomachenko, Zhi Su,* Yong Qian, Martin J. Paterson,* Zong-Wan Mao,* Hong-Ke Liu,* and Peter J. Sadler*

Cite This: *Inorg. Chem.* 2021, 60, 17450−17461 Read Online

ACCESS | Metrics & More | Article Recommendations | Supporting Information

ABSTRACT: Half-sandwich Os-arene complexes exhibit promising anticancer activity, but their photochemistry has hardly been explored. To exploit the photocytotoxicity and photochemistry of Os-arenes, *O,O*-chelated complexes [Os(η^6-*p*-cymene)(Curc)Cl] (**OsCUR-1**, Curc = curcumin) and [Os(η^6-biphenyl)(Curc)Cl] (**OsCUR-2**), and *N,N*-chelated complexes [Os(η^6-biphenyl)(dpq)-I]PF_6 (**OsDPQ-2**, dpq = pyrazino[2,3-*f*][1,10]phenanthroline) and [Os(η^6-biphenyl)(bpy)I]PF_6 (**OsBPY-2**, bpy = 2,2′-bipyridine), have been investigated. The Os-arene curcumin complexes showed remarkable photocytotoxicity toward a range of cancer cell lines (blue light IC_{50}: 2.6−5.8 μM, photocytotoxicity index PI = 23−34), especially toward cisplatin-resistant cancer cells, but were nontoxic to normal cells. They localized mainly in mitochondria in the dark but translocated to the nucleus upon photoirradiation, generating DNA and mitochondrial damage, which might contribute toward overcoming cisplatin resistance. Mitochondrial damage, apoptosis, ROS generation, DNA damage, angiogenesis inhibition, and colony formation were observed when A549 lung cancer cells were treated with **OsCUR-2**. The photochemistry of these Os-arene complexes was investigated by a combination of NMR, HPLC-MS, high energy resolution fluorescence detected (HERFD), X-ray adsorption near edge structure (XANES) spectroscopy, total fluorescence yield (TFY) XANES spectra, and theoretical computation. Selective photodissociation of the arene ligand and oxidation of Os(II) to Os(III) occurred under blue light or UVA excitation. This new approach to the design of novel Os-arene complexes as phototherapeutic agents suggests that the novel curcumin complex **OsCUR-2**, in particular, is a potential candidate for further development as a photosensitizer for anticancer photoactivated chemotherapy (PACT).

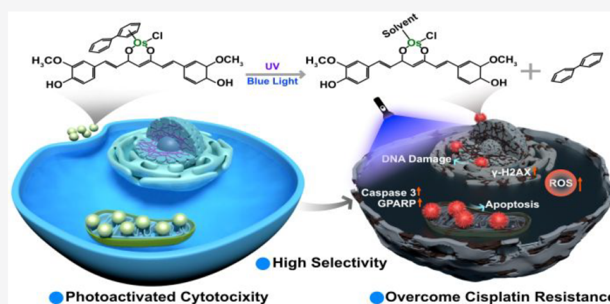

Downloaded via MOSCOW STATE UNIV on May 12, 2026 at 13:38:45 (UTC).
See https://pubs.acs.org/sharingguidelines for options on how to legitimately share published articles.

■ INTRODUCTION

Encouraged by the "from bench to clinic" story of platinum anticancer drugs, the study of other transition metals as anticancer agents has become a rapidly expanding field.[1−3] For example, complexes of Group 8 metals iron, ruthenium, and osmium have shown promising anticancer activity *in vitro* and *in vivo*.[4−6] Photoactivatable complexes are attractive because of their potential ability to minimize effects on normal tissue through the use of light directed to the tumor. These complexes only exert high antitumor activity under light irradiation while being inactive in the dark, which can minimize side effects on normal cells and tissues.[6] Ru- and Ir-based complexes have been well studied especially as polypyridine-type complexes, some of which have high anticancer activity. The photochemistry of Os-arene complexes and their potential for use in phototherapy have hardly been investigated.

Very few Os-arene complexes are known to photodissociate the arene ligand in preference to their mono- or bidentate ligands.[6,7] Based on this observation, two strategies for the design of Os-based photoactivated anticancer agents can be envisaged: (i) photosubstitution of Os-bound ligands by important biomolecules such as nucleobases, and (ii) photoredox reactions at the Os center to induce oxidative damage to cancer cells. Such Os-arenes might then have potential in photoactivated chemotherapy (PACT) or photodynamic therapy (PDT).[8,9]

Osmium(II) arene complexes with *N,N*-chelating ligands, such as [Os(arene)(N−N)I]$^+$, can exhibit potent anticancer activity *in vitro* and *in vivo*,[10−20] and *O,O*-chelated curcumin complexes also have good anticancer potency. To date, 12 metal-arene based curcumin complexes have been reported with moderate anticancer cytotoxicity (Table S1), but their phototoxicity and anticancer mechanisms have not been explored.[13−20] Curcumin (1,7-bis(4-hydroxy-3-methoxyphenyl)-1,6-heptadiene-3,5-dione, CurcH) has attracted much

Received: January 25, 2021
Published: September 9, 2021

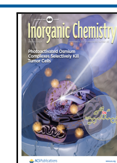

© 2021 American Chemical Society

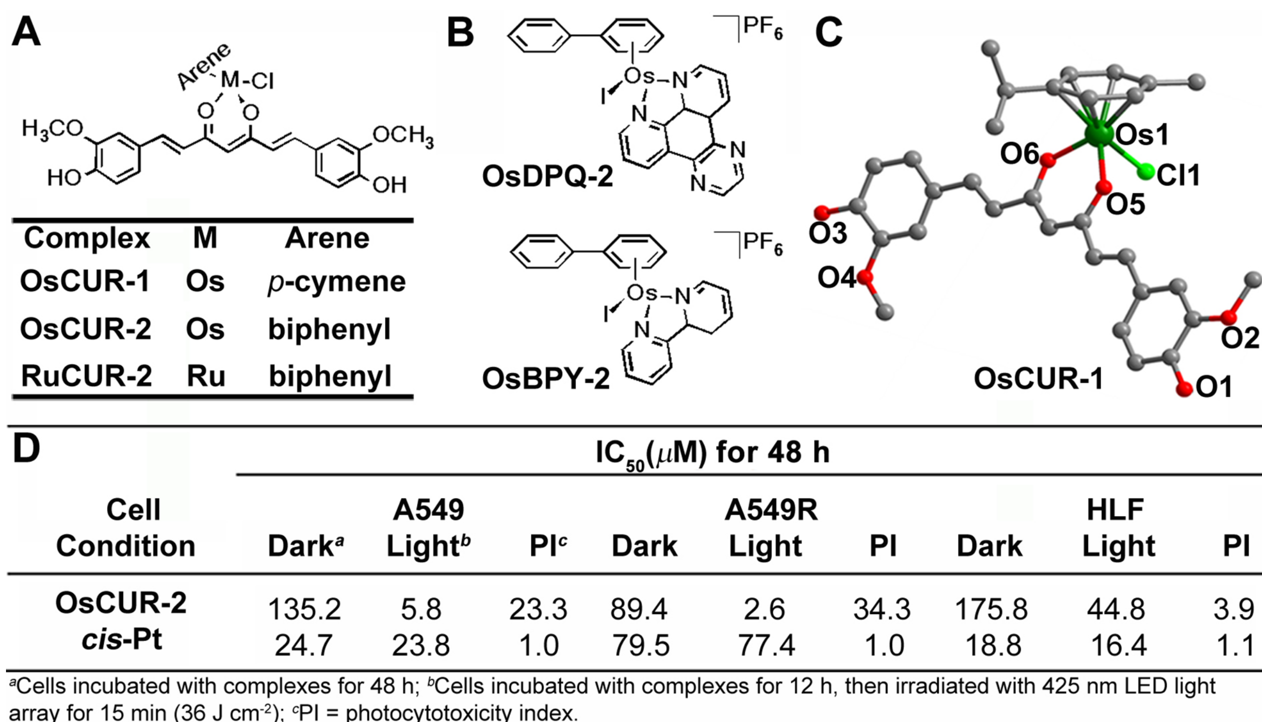

Cell Condition	A549 Dark[a]	A549 Light[b]	A549 PI[c]	A549R Dark	A549R Light	A549R PI	HLF Dark	HLF Light	HLF PI
	IC_{50}(μM) for 48 h								
OsCUR-2	135.2	5.8	23.3	89.4	2.6	34.3	175.8	44.8	3.9
cis-Pt	24.7	23.8	1.0	79.5	77.4	1.0	18.8	16.4	1.1

[a]Cells incubated with complexes for 48 h; [b]Cells incubated with complexes for 12 h, then irradiated with 425 nm LED light array for 15 min (36 J cm^{-2}); [c]PI = photocytotoxicity index.

Figure 1. (A,B) Molecular structures of **OsCUR-1**, **OsCUR-2**, **RuCUR-2**, **OsDPQ-2**, and **OsBPY-2**. (C) X-ray crystal structure of **OsCUR-1**, where the hydrogen atoms and PF_6^- are omitted for clarity. (D) IC_{50} values (μM) of complexes **OsCUR-2** and cisplatin (*cis*-Pt) toward various cell lines for 48 h treatment.

attention for therapy, due to its multifunctionalities in inhibiting carcinogenesis and limiting tumor growth.[19,20] Moreover, curcumin is a photosensitizer which absorbs visible light (400−500 nm), and itself is a candidate photodynamic therapy (PDT) agent.[19] Despite exhibiting interesting anticancer activity, curcumin (CurcH) still has limited utility because of its low bioavailability and hydrolytic instability under physiological conditions.[19,20] As a result, metal curcumin complexes have been explored as a means of avoiding the hydrolysis of the diketone through formation of coordination bonds, including complexes of Pt(II), Zn(II), Cu(II), and Ga(III).[19−23]

Herein, we report the synthesis and characterization of *O,O*-chelated Os(II) complexes [Os(η^6-*p*-cymene)(Curc)Cl] (**OsCUR-1**) and [Os(η^6-biphenyl)(Curc)Cl] (**OsCUR-2**) and for comparison Ru(II) complex [Ru(η^6-biphenyl)(Curc)-Cl] (**RuCUR-2**) and *N,N*-chelated [Os(η^6-biphenyl)(dpq)I]-PF_6 (**OsDPQ-2**, dpq = pyrazino[2,3-*f*][1,10]phenanthroline) and [Os(η^6-biphenyl)(bpy)I]PF_6 (**OsBPY-2**, bpy = 2,2′-bipyridine). The structure of **OsCUR-1** was determined by single-crystal X-ray diffraction. The photocytotoxicity and anticancer mechanism of these Os-arene complexes were studied by a range of chemical and physical techniques and cell biological assays, including the MTT colorimetric cytotoxicity assays, confocal microscopy, ICP-MS analysis, flow cytometry, Western blotting, comet assays, colony formation, and HUVECs tube formation assays. The photochemistry of the complexes was investigated by various techniques including high-energy resolution fluorescence detected (HERFD) X-ray adsorption near-edge structure (XANES)[24] and total fluorescence yield (TFY) XANES spectroscopy,[25] UV−vis, fluorescence, and NMR spectroscopy, HPLC-MS, and theoretical computation. Selective photodissociation of the π-bound arene ligand and oxidation of the Os(II) center were investigated for excitation by UVA and blue light.

■ RESULTS

Synthesis. All Os complexes were prepared by a general one-step reaction of the Os-arene dimers [Os(arene)X_2]$_2$ (arene = biphenyl or *p*-cymene, X = Cl or I) with a chelating ligand (details in Supporting Information, Experimental Section, Figure 1, Scheme S1). The Ru complex **RuCUR-2** was synthesized for comparison. The purity of all complexes was determined to be ≥95% by NMR and elemental analysis. Single-crystal diffraction of **OsCUR-1** revealed the classical piano-stool structure with the *O,O*-donor curcumin chelated to Os in the {Os(η^6-*p*-cymene)Cl} unit, and the monomers were further connected through hydrogen bonds and $\pi-\pi$ interactions (Tables S2−S4, Figures 1, S1, and S2). The structure of **OsCUR-1** is very similar to that of [Ru(η^6-*p*-cymene)(Curc)Cl][15] and bis((1,7-bis(3,4-dimethoxyphenyl)-hept-1,6-diene-3,5-dione)-(η^6-*p*-cymene)chlororuthenium-(II),[16] with bond lengths in similar ranges. An isostructural complex [Os(η^6-*p*-cymene)(Curc)Cl] was reported recently by Dyson et al., crystallized in the orthorhombic space group *Pbca*, in contrast to the monoclinic *C*2/*c* space group observed here.[17]

Cytotoxicity and Photocytotoxicity. The *in vitro* anticancer activity of complexes **OsDPQ-2** and **OsBPY-2** was investigated. **OsDPQ-2** showed good anticancer activity in the dark, with an IC_{50} value of 2 μM, similar to cisplatin under the same experimental conditions (Chart S1). However, **OsBPY-2** is inactive, IC_{50} > 50 μM. The distribution of Os in A2780 human ovarian cancer cells was studied after incubation with 4 μM **OsDPQ-2**. The Os content in four fractions, cytosol, membrane plus particulate fraction, nucleus, and cytoskeleton, was determined by ICP-MS. Most of the Os

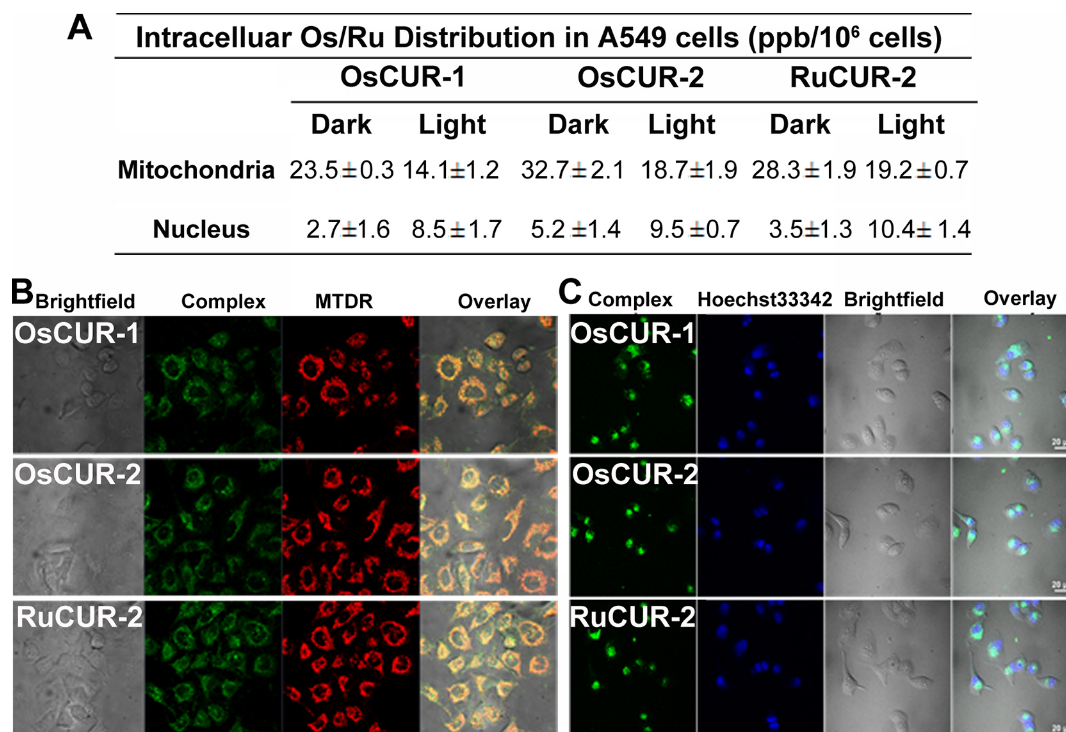

A

Intracelluar Os/Ru Distribution in A549 cells (ppb/10⁶ cells)

	OsCUR-1		OsCUR-2		RuCUR-2	
	Dark	Light	Dark	Light	Dark	Light
Mitochondria	23.5±0.3	14.1±1.2	32.7±2.1	18.7±1.9	28.3±1.9	19.2±0.7
Nucleus	2.7±1.6	8.5±1.7	5.2±1.4	9.5±0.7	3.5±1.3	10.4±1.4

Figure 2. (A) Intracellular Os and Ru distribution in A549 cells incubated with 10 μM **OsCUR-1**, **OsCUR-2**, or **RuCUR-2** for 12 h in the dark or light (photoirradiation for 15 min and then dark incubation for 11 h 45 min) determined by ICP-MS (ppb/10^6 cells). (B,C) Confocal fluorescence microscopy images of A549 cells treated with complexes **OsCUR-1**, **OsCUR-2**, and **RuCUR-2**, before (B) and after photoirradiation (C), showing that the complexes are accumulated in the mitochondria and nucleus, respectively. The excitation wavelength was 460 nm, with emission at 500–600 nm.

(80%) was in the membrane plus particulate fraction, and 10% was in the nucleus (Figure S3). To examine whether **OsDPQ-2** in the membranes affected the cell cycle progression of A2780 cells, a further cell cycle analysis was performed after incubation with varying concentrations of **OsDPQ-2** for 24 h (1, 5, and 20 μM). These experiments revealed that S-phase cell cycle arrest was induced by **OsDPQ-2** (Figure S4).

To test the potential for using Os arene compounds as phototherapeutic agents, **OsCUR-1** and **OsCUR-2** (controls: **RuCUR-2**, curcumin, and cisplatin) were assessed against a panel of human cell lines: lung carcinoma A549, cisplatin-resistant A549R, breast cancer MCF-7, cervical cancer HeLa, liver cancer HepG2, normal lung HLF, and liver LO2 cell lines, as shown in Figure 1D and Table S27. Significant phototoxicity upon irradiation was observed for these osmium compounds, with higher potency toward cisplatin-resistant A549R cancer cells and high selectivity for cancer cells over normal cells. The biphenyl Os(II) complex **OsCUR-2** exhibited the highest phototoxicity, the highest PI values, and selectivity toward both the cisplatin-resistant A549R cells and A549 cells. For example, **OsCUR-2** is relatively noncytotoxic in the dark (IC_{50}: 73−135 μM) toward all tested cells. Upon irradiation, the phototoxicity IC_{50} decreased to 5.8 and 2.6 μM with PI values of 23.3 and 34.4 against A549 and A549R cancer cells, respectively, while the IC_{50} value was 44.8 μM for normal HLF cells (relatively nontoxic). The selectivity factor for A549R cells was up to 17.2-fold compared with normal HLF cells upon irradiation. Curcumin itself displayed moderate cytotoxicity against A549 cancer cells and HLF normal cells in the dark, showing no selectivity for lung cancer cells over normal lung cells. As expected, cisplatin exhibited little photocytotoxicity toward the tested cells under these conditions.

Subcellular Localization in the Dark or upon Irradiation. The subcellular localization of **OsCUR-1**, **OsCUR-2**, **RuCUR-2**, and curcumin in A549 cells was investigated by confocal microscopy (Figures 2 and S5) without photoirradiation. Green luminescence of **OsCUR-1**, **OsCUR-2**, **RuCUR-2**, or curcumin was observed within 1 h, suggesting significant cellular uptake of **OsCUR-1**, **OsCUR-2**, **RuCUR-2**, and curcumin in the cytoplasm (Figure S5). High Pearson's colocalization coefficients were obtained by confocal microscopy for **OsCUR-1**, **OsCUR-2**, **RuCUR-2**, and curcumin with the mitochondria-specific probe MitoTracker Deep Red (MTDR), implying that nearly 90% of these complexes were observed to be in the mitochondria (Figure 2B). The ICP-MS data also suggested that in the dark most of the Os-arene or Ru-arene curcumin complexes were located in the mitochondria and cytoplasm (Figure 2A).

Redistribution of the metal-arene complexes after photoirradiation was also revealed by confocal microscopy and ICP-MS. In the confocal images of pretreated A549 cells after photoirradiation and incubation for another 12 h, the intense green luminescence of the metal-arene complexes emerged in A549 cells and exhibited a partially overlapping profile with the fluorescence of nucleus dye 2′-(4-ethoxyphenyl)-5-(4-methyl-1-piperazinyl)-2,5′-bi-1*H*-benzimidazole trihydrochloride (Hoechst 33342, Figure 2C). Since the metal centers remained coordinated to curcumin after the irradiation, the observation of luminescence in the nucleus suggested more Os/Ru-Cur fragments had accumulated in the nucleus after the irradiation. The ICP-MS data also indicated that the content of Os/Ru dramatically increased in the nucleus, accompanied by a decrease in the mitochondria after the irradiation (Figure 2A). For example, the Os content of **OsCUR-2** in A549 cells

https://doi.org/10.1021/acs.inorgchem.1c00241
Inorg. Chem. 2021, 60, 17450−17461

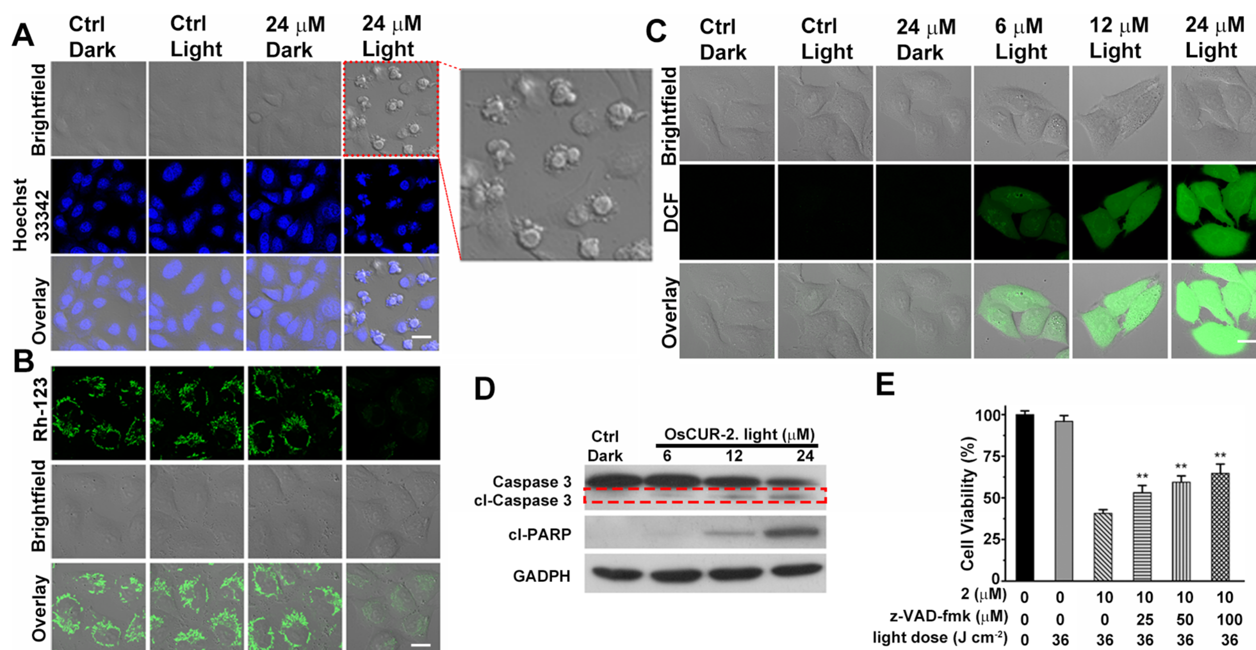

Figure 3. Characterization of apoptosis for A549 cancer cells treated with **OsCUR-2** under photoirradiation (425 nm LED light for 15 min, 36 J cm^{-2}): (A) morphological observations with Hoechst 33342 staining. (B) MMP ($\Delta\Psi_m$) analysis stained with Rh-123. (C) Observation of ROS generation with the probe DCFH-DA by confocal microscopy during **OsCUR-2**-mediated photocytotoxicity (425 nm LED light for 15 min, 36 J cm^{-2}). (D) Western blotting analysis of the indicated proteins from A549 cells in the dark and after treatment with various concentrations of **OsCUR-2** and photoirradiation. (E) Concentration-dependent inhibition of z-VAD-fmk on cell death induced by **OsCUR-2**-mediated photocytotoxicity toward A549 human lung cancer cells. Data are represented as means ± SD of three independent experiments. **, $P < 0.01$, as compared with the group treated with **OsCUR-2** (10 μM) in the absence of z-VAD-fmk. Scale bar = 40 μm.

dropped from 32.7 to 18.7 ppb/10^6 cells in the mitochondria but increased from 5.2 to 9.5 ppb/10^6 cells in the nucleus after the irradiation, in agreement with the confocal images.

Apoptosis. Upon irradiation, **OsCUR-2** exhibited the highest photocytotoxicity toward A549 human lung cancer cells and cisplatin-resistant A549R lung cancer cells; thus, A549 cells were chosen for exploration of the mechanism of the phototoxicity. Apoptosis is one of the most common cell death pathways, accompanied by cell shrinkage, nuclear fragmentation, membrane blebbing, and apoptotic body formation.[26] To verify whether **OsCUR-2** induced apoptosis in A549 cells upon irradiation, the morphological changes in A549 cells were first examined by staining with Hoechst 33342.[27] As shown in Figure 3A and Figure S14A, upon irradiation with **OsCUR-2**, apoptosis-induced morphological features were observed with an increasing dependence on concentration, including plasma membrane blebbing, fragmented nuclei, and apoptotic bodies. In contrast, the control cells (both in the dark with or without **OsCUR-2** and in the light without **OsCUR-2**) displayed normal morphology with round and homogeneous nuclei. Apoptosis also results in the depolarization of the mitochondria and a decrease in the mitochondrial membrane potential (MMP, $\Delta\Psi_m$) of the cells.[28] Rhodamine 123 (Rh-123) was used to investigate the MMP by confocal microscopy, since it is readily washed out once the MMP is lost. Green fluorescence of Rh-123 was detected in A549 cells after incubation with **OsCUR-2** upon irradiation (Figure 3B and Figure S14B), suggesting that the cancer cells maintained their viability. The $\Delta\Psi_m$ showed a marked decreasing trend as revealed by the fluorescence intensity with increasing concentrations of **OsCUR-2** upon irradiation.

Caspase-3 plays a decisive role in the execution of apoptosis and is responsible for the cleavage of PARP during cell death.[29] As compared with control cells in the dark, dose-independent increases in cleaved-caspase-3 and cleaved-PARP (clPARP) activities were detected in A549 cells treated with **OsCUR-2** upon light irradiation (Figure 3D). Moreover, z-VAD-fmk, a pan-caspase inhibitor, efficiently attenuated cell death caused by photoactivated **OsCUR-2** (Figure 3E). In the presence of z-VAD-fmk (100 μM), the cell viability increased from 40.7% to 64.7% when cells were treated with **OsCUR-2** (10 μM) and irradiated by blue light, 425 nm. These data suggest that photoactivated **OsCUR-2** kills A549 cells mainly via apoptosis, through caspase-dependent mechanisms.

ROS Generation. Generation of reactive oxygen species (ROS) is the main mechanism responsible for photosensitizer-induced cell death.[30] The ability of **OsCUR-2** to generate ROS within A549 cells was investigated using the ROS probe, 2′,7′-dichlorofluorescein diacetate (DCF-DA).[31] Upon light irradiation, the intensity of green intracellular fluorescence from **OsCUR-2** in A549 cells increased significantly in a concentration-dependent manner (Figure 3C), indicating the generation of ROS. Flow cytometric analysis further confirmed that a 9-fold increase in the ROS probe signal intensity was observed in A549 cells treated with **OsCUR-2** (25 μM) under light irradiation as compared with the control cells treated with **OsCUR-2** in the dark alone (Figure S6).

DNA Damage. The expression level of γ-H2AX, an established molecular marker of DNA damage, and one of the major and early cellular responses to the induction of nuclear foci, was determined for A549 cells after treatment with **OsCUR-2** upon irradiation and analyzed by immunofluorescence analysis and Western blotting.[32] γ-H2AX

https://doi.org/10.1021/acs.inorgchem.1c00241
Inorg. Chem. 2021, 60, 17450−17461

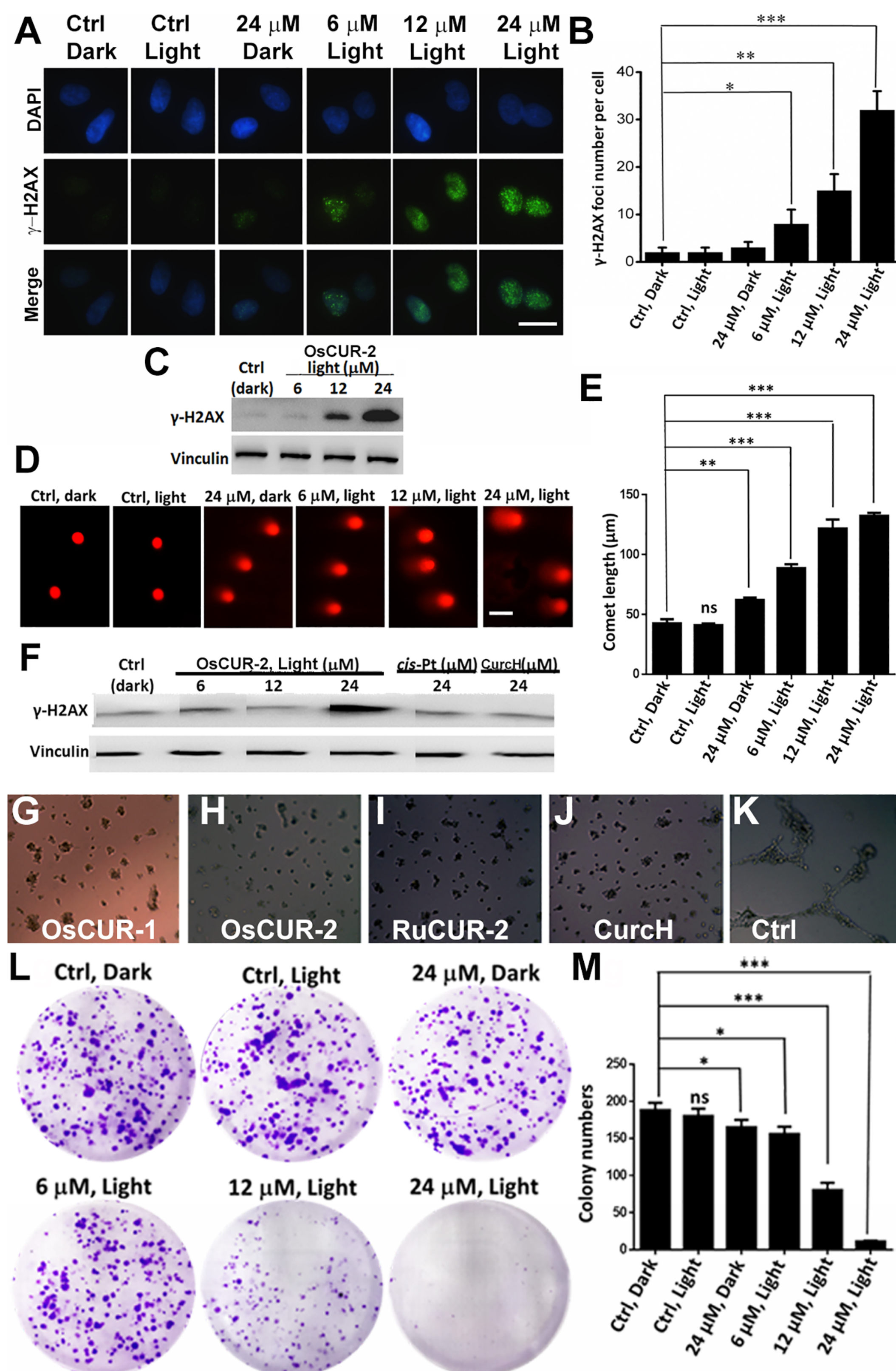

Figure 4. (A) Cell immunostaining assay, (B) statistical quantification, and (C) Western blotting of the expression level of γ-H2AX of A549 cells after the treatment of **OsCUR-2** under irradiation. *, $P < 0.05$, **, $P < 0.01$, ***, $P < 0.001$. Scale bar = 40 μm. (D) and (E) fluorescence images and statistical quantification obtained from an alkaline comet assay for A549 cells on preincubation for 4 h with complex **OsCUR-2** with or without irradiation. Scale bar = 10 μm. (F) Western blotting of the expression level of γ-H2AX of cisplatin-resistant A549R cells after the treatment of **OsCUR-2**, *cis*-Pt, or CurcH under irradiation. The irradiation was 425 nm LED light for 15 min, 36 J cm^{-2}. (G−K) *In vitro* antiangiogenic activity of listed complexes (5 μM) and the control on HUVECs. (L,M) Images of colony formation and statistic quantification of A549 cells after treatment with **OsCUR-2** with or without photoirradiation (425 nm LED light for 15 min, 36 J cm^{-2}). ns, not significant. **, $P < 0.01$. ***, $P < 0.001$.

https://doi.org/10.1021/acs.inorgchem.1c00241
Inorg. Chem. 2021, 60, 17450−17461

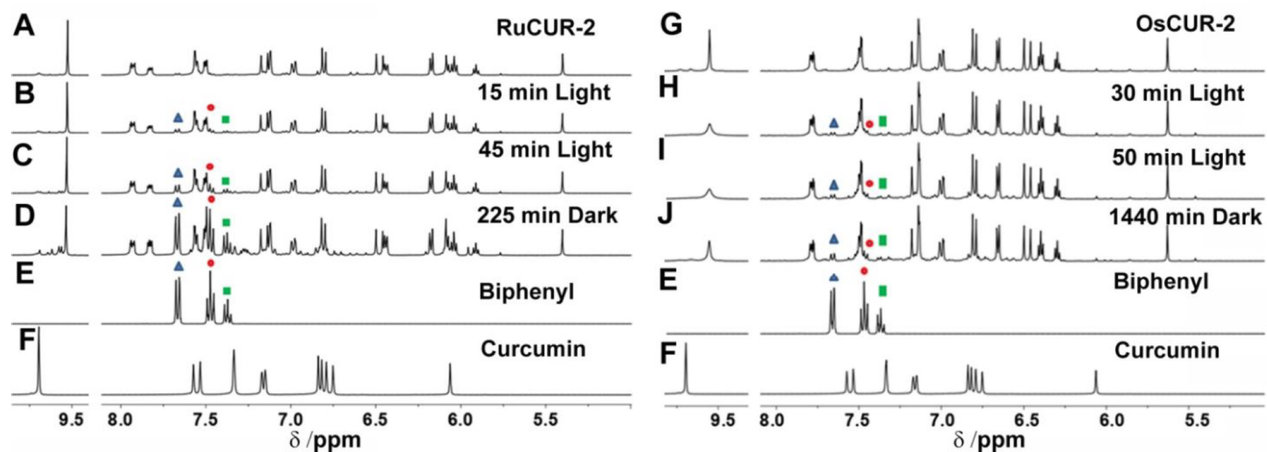

Figure 5. ^{1}H NMR spectra of **RuCUR-2** (A−D) and **OsCUR-2** (G−J) (100 mM, DMSO-d_6) before and after photoirradiation (425 nm, 100 mW) together with ^{1}H NMR spectra of biphenyl (E) and curcumin (F). (A and G) initial complexes, (B,C and H,I) after irradiation for specific times, and (D or J) following a rest in the dark for another 180 min for **RuCUR-2** or 1390 min for **OsCUR-2**. Triangles, circles, and squares denote the signals of released biphenyl.

expression was significantly elevated in a dose-independent manner in A549 cells after the treatment (Figure 4A−C), suggesting the photoactivity of **OsCUR-2** enhances the frequency of DNA double-strand breaks (DSBs). The expression levels of γ-H2AX in cisplatin-resistant A549R cells after the treatment with **OsCUR-2**, *cis*-Pt, or CurcH under irradiation are shown in Figure 4F. Significantly elevated γ-H2AX expression was observed only for **OsCUR-2**, while those for cisplatin and CurcH remained unchanged. This indicated that effective DNA damage in cisplatin-resistant cells was caused by **OsCUR-2**, which may contribute to overcoming cisplatin resistance.

A single cell gel electrophoresis assay (SCGC, comet assay), commonly used to detect cellular DNA damage as single-strand breaks, was also used.[33] As seen in Figure 4D,E, the length of the comet dramatically increased compared to the control samples (∼2.5-fold longer), and differently sized and fragmented dead cells were observed after treatment with **OsCUR-2** upon irradiation. In contrast, the control samples exhibited almost condensed nuclei. The comet length for **OsCUR-2**-treated A549 cells in the dark elongated only slightly, which indicated much less DNA damage in the dark than that after photoirradiation. The results of the comet assay illustrate that the DNA double helix has been at least partially denatured and that some nuclear DNA becomes single stranded upon photoirradiation with **OsCUR-2** treatment.

Angiogenesis and Colony Formation. The effects of **OsCUR-1**, **OsCUR-2**, and **RuCUR-2** on angiogenesis were studied by using human umbilical vein endothelial cells (HUVECs) (Figure 4G−K).[34] These complexes, as well as curcumin itself, exhibited antiangiogenic activity. In addition, the colony formation assay confirmed the antiproliferative activity, invasiveness, sensitivity, and long-term toxic effect of **OsCUR-2** upon irradiation with A549 cells (Figure 4L,M). Colony formation by A549 cells was significantly inhibited after a two-week incubation with **OsCUR-2** upon irradiation in a dose-independent manner. There was less than 1% of survival of A549 cells after **OsCUR-2** treatment and photoirradiation at a concentration of 24 μM. In contrast, more than 95% of A549 cancer cells survived after treatment without **OsCUR-2** both in the dark and after photoirradiation. These results suggest that **OsCUR-2** can efficiently inhibit angiogenesis and colony formation and might have the potential to suppress tumor metastasis.

Optical Properties. Both **OsCUR-1** and **OsCUR-2** show intense absorption at 425 nm, while **RuCUR-2** has an intense band at 408 nm with a shoulder at 445 nm (Figure S7). Furthermore, both **RuCUR-2** and **OsCUR-2** exhibit maximum emissions at 545 or 560 nm, close to that of curcumin itself (548 nm) with excitation in the range of 450−461 nm. The maximum emission of **OsCUR-1** is significantly blue-shifted to 507 nm with excitation at 461 nm (Figure S8 and Table S5). The dramatic difference between **OsCUR-1** and **OsCUR-2** can be ascribed to the different arene groups, *p*-cymene vs biphenyl. The UV−vis spectra of **OsDPQ-2** and **OsBPY-2** are similar (Figure S9). **OsDPQ-2** has absorption maxima at 280 nm, 300 nm (shoulder), 420 nm, and 500 nm (shoulder). After irradiation of **OsDPQ-2** and **OsBPY-2** by UVA (365 nm), UV−vis spectra were recorded at various time intervals over the course of 4 h. The absorption intensity at 280 and 420 nm decreased, while that at 500 nm increased (Figure S9).

Biphenyl Photodissociation Studied by ^{1}H NMR and LC-MS. Time-dependent ^{1}H NMR was used to monitor the photoirradiation reactions of **OsCUR-2**, **RuCUR-2**, **OsDPQ-2**, and **OsBPY-2** with blue light (425 nm) or UVA (365 nm) at ambient temperature (Figures 5 and S12). After irradiation for 50 or 45 min, new peaks at 7.66, 7.47 and 7.37 ppm were observed for **OsCUR-2** or **RuCUR-2**, which can be assigned to the free biphenyl ligand. The intensities of these peaks increased when the samples were kept in the dark after irradiation. These results implied that the biphenyl arene was released after photoirradiation of **OsCUR-2** and **RuCUR-2**. However, it was notable that no new set of signals for other photoproducts from **OsCUR-2** and **RuCUR-2** such as metal-curcumin fragments was observed.

Similar results were observed for ^{1}H NMR experiments when **OsDPQ-2** and **OsBPY-2** were photoirradiated by either blue light (425 nm) or UVA (365 nm). However, ^{1}H NMR signals disappeared after irradiation for 1 or 2 h. Then, the biphenyl photodissociation reaction was further studied by LC-MS experiments. Only one LC peak was observed at 17.2 min with m/z of 705.0276 before irradiation, attributable to $[Os(\eta^6\text{-bip})(dpq)I]^+$, but two new LC peaks appeared at 18.6 and 19.5 min with m/z of 582.9697 and 552.9572 with

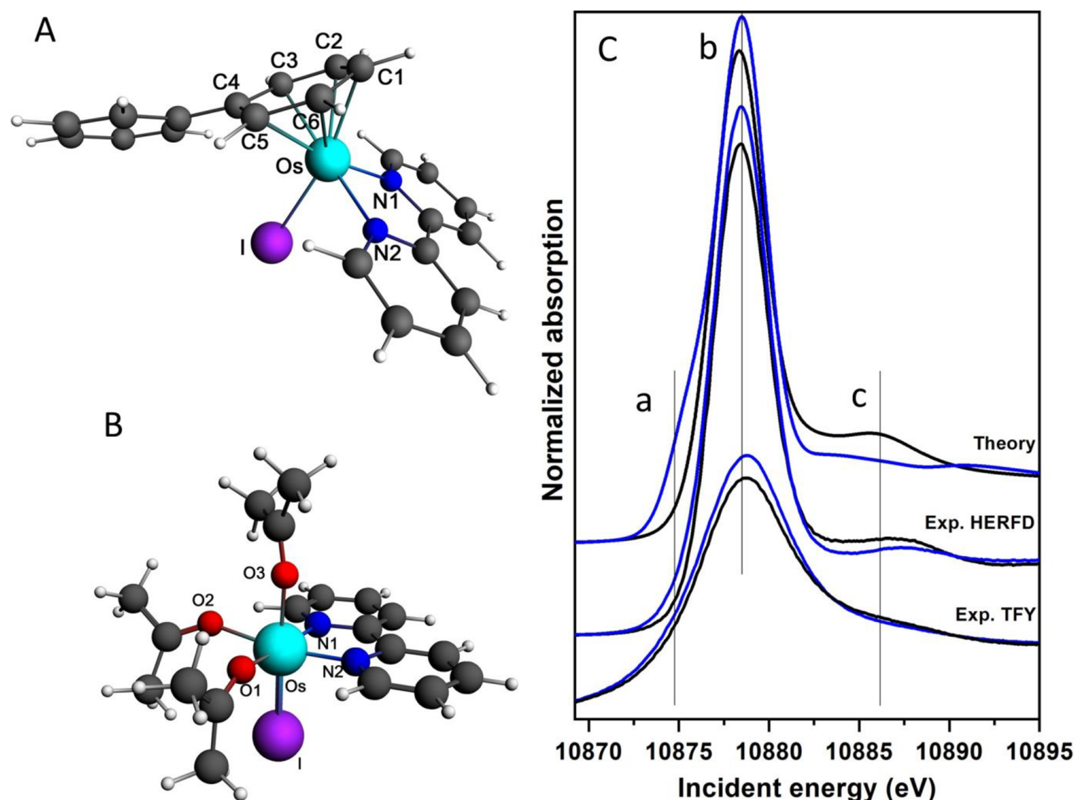

Figure 6. DFT optimized structures of (A) **OsBPY-2** before light irradiation and (B) its putative photoproduct $[Os(bpy)(acetone)_3I]^{2+}$. (C) Experimental and calculated X-ray absorption spectra of the **OsBPY-2** in acetone solution before (black line) and after (blue line) irradiation with blue light. Shift along the vertical axis is for the sake of clarity.

characteristic Os isotopic peaks after irradiation for 4 h, assignable to biphenyl-depleted **OsDPQ-2** ($[Os(dpq)I + 2H]^+$ and $[Os(dpq)I^+ + MeOH]$), respectively, further confirming the loss of biphenyl from **OsDPQ-2** after the irradiation (Figure S13).

It was remarkable that during the photoreaction, ^{1}H NMR peaks corresponding to the initial **OsBPY-2** disappeared over ~2 h, and the only peaks visible in the spectrum were for free biphenyl (Figure S12). The photodecomposition reaction of **OsBPY-2** was further investigated by X-ray absorption spectroscopy, a powerful technique to investigate local geometry and electronic structure of metal ions in organometallic compounds.[35] We acquired the Os L_3-edge HERFD-(High Energy Resolution Fluorescence Detected) and TFY (Total Fluorescence Yield) XANES (X-ray Absorption Near Edge Structure) spectra of initial and light-irradiated **OsBPY-2** at the ID26 beamline of the ESRF synchrotron, following previously described procedures.[36] Experimental Os L_3-edge HERFD and TFY XANES of the **OsBPY-2** and light-irradiated **OsBPY-2** together with the theoretical spectrum are shown in Figure 6. The resolution gain of the HERFD spectrum compared to the TFY is clearly visible. Calculated XANES spectra were in good agreement with the experiment, confirming the reliability of the structural model obtained. The changes occurring in the experimental XANES spectra upon irradiation of the sample with blue light are qualitatively reproduced by the theory in the pre-edge (a), white line (b), and postedge (c) spectral regions. Notably, changes in the conventional TFY XANES are much smaller, which would have made the analysis much more difficult without the high-resolution data.

To analyze the spectra (see SI Section Experimental Procedures for details), we modeled the structure of a putative photoproduct taking into account the loss of the biphenyl ligand and the formation of an octahedral Os center coordinated to three solvent molecules (acetone, as $[Os(bpy)(acetone)_3I]^{2+}$), Figure 6B. The good agreement between the calculated and experimental XANES spectra overall confirms the generation of an Os(III) center upon light irradiation of **OsBPY-2**.

■ DISCUSSION

We have studied the photochemistry, phototoxicity, and anticancer mechanism of action of half-sandwich Os(II) arene complexes containing the *O,O*-chelating and *N,N*-chelating ligands, together with chloride or iodide as a monodentate ligand. Very few studies of photoactivatable osmium complexes have been reported so far. Brewer et al. reported the inhibition of growth of African green monkey kidney epithelial (Vero) cells by an osmium bipyridine complex $[\{(bpy)_2Os(dpp)\}_2RhCl_2]Cl_5$ [bpy = 2,2′-bipyridine; dpp = 2,3-bis(2-pyridyl)pyrazine].[6] The current work appears to be the first study of the photochemistry and photobiology of half-sandwich Os(II) complexes.

Phototoxicity, Cellular Distribution, and Anticancer Mechanism. The Os/Ru-arene curcumin complexes **OsCUR-1**, **OsCUR-2**, and **RuCUR-2** exhibited low dark toxicity toward both cancer and normal cell lines, but showed potent phototoxicity toward cancer cell lines after irradiation, especially toward the cisplatin-resistant A549R human lung cancer cells. This high phototoxicity suggests that Os-arene curcumin complexes might be promising candidates as

photochemotherapeutic agents and overcome cisplatin resistance.[37,38] The phototoxicity of the biphenyl complex **OsCUR-2** is the highest among the three metal-arene curcumin complexes, perhaps reflecting the higher inertness of Os(II) compared to Ru(II).[39] **OsCUR-1**, **OsCUR-2**, and **RuCUR-2** localized mainly in the mitochondria of A549 cells without irradiation; the same cellular localization was also observed for previously reported curcumin metal complexes, such as V(IV) and Nb(III),[19−21,28] indicating that after coordination with metal centers, curcumin retains its ability to target mitochondria.[22] The apoptosis-induced morphological features, a decrease in the mitochondrial membrane potential (MMP, $\Delta\Psi_m$) together with increases in cleaved-caspase-3 and cleaved-PARP (clPARP) activities, suggested that these photoactivated Os-arene complexes kill cancer cells via apoptosis through caspase-dependent mechanisms (Figure 3). A 9-fold increase in the ROS signal intensity, antiangiogenic activity, and significant inhibition of colony formation were also observed, indicating a multitargeting anticancer mechanism of action.

Activity in Cisplatin-Resistant Cells. Mitochondria were damaged in A549R cells after photoirradiation and Os partially migrated to the nuclei (Figure 2). Both mitochondrial damage and translocation of Os from the mitochondria to nuclei after photoirradiation could lead to the DNA damage. A significantly elevated expression level of γ-H2AX upon irradiation of A549R cells treated with **OsCUR-2** was observed, while for cisplatin or curcumin, the level remained unchanged, indicative of DNA damage in A549R cells caused by **OsCUR-2**. Furthermore, the comet assay illustrated that the DNA double helix in A549R cells was partially denatured, and the nuclear DNA became single stranded upon photoirradiation with **OsCUR-2** (Figure 4). These results indicated that irradiated **OsCUR-2** overcomes cisplatin resistance via mitochondrial and DNA damage.

Computational Studies of Photophysical Properties. DFT calculations were carried out for the Os-arenes (Figure S11, Tables S6−S23).[40] Singlet state TDDFT calculations were run in aqueous solutions (cpcm method) to assign the absorption bands in the electronic spectrum.[41,42] The computed electronic transitions for **OsCUR-1**, **OsCUR-2**, and **RuCUR-2** indicate maxima at 444, 445, and 456 nm (Tables S7, S12, and S17), respectively, consistent with experimental results. The orbital energies for the HOMO and LUMO are listed in Table S6. The UV absorption for **OsCUR-1** is mainly due to an S0 → S3 electronic transition, and analysis of the Natural Transition Orbitals (NTOs) clearly shows the MLCT character in this transition (Table S9). The photoluminescence emission for **OsCUR-1** is due to the intraligand charge transfer (ILCT) according to the NTO analysis[43a] (Tables S8−S11). Similarly, the UV−vis absorptions of **OsCUR-2** and **RuCUR-2** are ascribed to the MLCT S0 → S1/S2 electronic transitions for **OsCUR-2** and S0 → S2 electronic transition for **RuCUR-2** (Tables S12−S19), with absorption maxima at 445 and 483 nm (shoulder), respectively (Figure S7). For **OsDPQ-2** (Tables S20−S23), the most intense band at 280 nm is due to mixed states of ^{1}MLCT and $^1\pi-\pi$ character according to the calculation,[43b] and the shoulder in the 300−350 nm region can be ascribed to ^{1}MLCT (Os, I → dpq) transitions; the lowest-energy bands are again of ^{1}MLCT type, involving different Os *d* orbitals. The agreement between the experimental spectra and the computed transitions is satisfactory, despite the underestimation of the oscillator strength relative to the lowest energy transition at 467 nm. This transition corresponds to the HOMO → LUMO transition.

Photoactivated Dissociation of the Arene Group and Oxidation of Os(II) upon Photoirradiation. Taube and coworkers reported that the Os-benzene dimer $[Os(\eta^6\text{-}C_6H_6)Cl_2]_2$ decomposes upon UVA (365 nm) irradiation, free benzene is released as a reaction product,[7] and arene photosubstitution reactions for Os(II) arene 1,4,7-trimethyl-1,4,7-triazacyclononane and 1,4,7-triazacyclononane complexes can be achieved after prolonged (>24 h) photolysis using UV irradiation (mercury arc lamp).[7] In our case, the photoactivated dissociation of the arene ligand was observed by ^{1}H NMR, LC-MS, HERFD, and TFY XANES techniques when these half-sandwich Os(II) biphenyl complexes were irradiated with UVA or blue light (Figures 6, S12, and S13) and also confirmed by DFT calculations. The released free biphenyl might further interact with DNA by intercalation and result in DNA damage. **RuCUR-2** exhibited a higher extent of biphenyl dissociation compared to **OsCUR-2** under similar irradiation conditions.[4]

On the other hand, the photodissociation may also result from the low-lying *dd* excited state, as all absorbing transitions include at least minor d-to-d character (Tables S9, S14, and S19). This is also supported by the fact that the *dd* component in **RuCUR-2** transitions is stronger than in **OsCUR-1** and **OsCUR-2** transitions, explaining a higher activity with **RuCUR-2**.[44]

The photoirradiation reactions of Os/Ru-arene curcumin complexes are different from that of the Pt(II)-curcumin complex $[Pt(Curc)(NH_3)_2](NO_3)$, in which the curcumin is released from the coordination complex.[22] The quantum yields for the photodissociation of biphenyl ligand from **RuCUR-2** and **OsCUR-2** were also determined, based on ^{1}H NMR data, which indicated that ∼50% and ∼9% biphenyl ligands had been released under the similar irradiation conditions from **RuCUR-2** and **OsCUR-2**, respectively. This result suggested that interaction between Ru(II) and the biphenyl was weaker than that for Os(II).

The release of the arene ligand from **OsDPQ-2** can be induced by photoirradiation with either blue light and UVA, and the iodido osmium complexes with bidentate ligands reported in this work appear to react much faster under irradiation. LC-MS data confirmed the release of the biphenyl ligand from **OsDPQ-2** after irradiation since two biphenyl-depleted species were detected. **OsDPQ-2** and **OsBPY-2** were studied to elucidate their photodecomposition pathways using DFT calculations (Tables S23 and S24). Geometry optimizations of **OsBPY-2** in the ground state (S0) and lowest-lying triplet state (T1) were performed in the gas phase, and the nature of all stationary points was confirmed by normal-mode analysis. The X-ray coordination bond lengths and angles around the Os center are listed in Tables S24 and S25.[41,42] The most dramatic difference is the weakened coordination between the Os center and the biphenyl arene group, where the Os−centroid bond length has elongated by 0.275 Å (from 1.767 to 2.042 Å) after the light irradiation, suggesting the dissociative character of the biphenyl arene group in **OsDPQ-2**. Several of the lowest energy transitions have contributions from the LUMO+3 and LUMO+4 orbitals, which have σ^* antibonding character toward the Os−I bond and partially also toward the Os−arene (Table S26). Such transitions therefore have partial dissociative character. The lowest-lying triplet and

two other triplet states of higher energy have dissociative character (Tables S15−S18), which were ^{3}MC[45,46] with the contributions from the same dissociative orbitals according to the spin density surface (Table S19). The nature and energy of the low-energy triplets is consistent with the lack of fluorescence from **OsDPQ-2** as well as its photochemical behavior.[43]

The photo-oxidation of Os(II) in **OsDPQ-2** and **OsBPY-2** was first revealed by ^{1}H NMR experiments. The ^{1}H NMR signals for **OsDPQ-2** disappeared when **OsDPQ-2** was photoactivated by blue light or UVA. Low-spin Os(II) (5d^6) is diamagnetic, and its complexes give sharp NMR peaks. In contrast, Os(III) is paramagnetic and expected to give very broad (even unobservable) peaks.[47]

The reactivity of **OsBPY-2** was investigated by HERFD and TFY XANES, and the structure of a putative photoproduct via loss of the biphenyl ligand and the formation of an octahedral Os center coordinating three solvent molecules (acetone) was modeled based on the experimental data (Figure 6). The emerging XANES pre-edge feature probably corresponds to a $2p \rightarrow t_{2g}$ transition, where the t_{2g} vacancy results from Os(II) oxidation. An analogous photoproduct $[(CH_3CN)_3Os(tacn)](PF_6)_2$ (where tacn = 1,4,7-triazacyclononane) has been isolated from the photolysis of $[(\eta^6$-*p*-cymene)Os(tacn)$](PF_6)_2$ in CH_3CN.[7] Experimental HERFD and TFY XANES of the nonirradiated **OsBPY-2** together with the theoretical spectrum are shown in Figure 6. The good agreement between the calculated and experimental XANES spectra overall confirmed the generation of an Os(III) center upon light irradiation of **OsBPY-2**. The formation of the photoproduct is due to the loss of an arene ligand and leads to an octahedral Os complex coordinated by solvent molecules, yet retaining the iodido and bpy ligands.

CONCLUSIONS

There are few reports of the photochemistry of Os(II) arene complexes. The Os(II) arene curcumin complexes **OsCUR-1** and **OsCUR-2**, studied here, exhibit high potent phototoxicity upon blue light irradiation, especially toward cisplatin-resistant cancer cell lines, and with high selectivity toward cancer cells. These complexes were translocated from mitochondria to the nucleus after irradiation, resulting in mitochondrial damage, apoptosis, ROS generation, DNA damage, angiogenesis inhibition, and colony formation. Even complex **RuCUR-2** with similar optical properties to those of **OsCUR-1** and **OsCUR-2** exhibited much lower cytotoxicity toward cancer cells compared to the Os complexes, due to the stronger heavy atom effect of Os compared to Ru. The photochemical reactions of these Os(II)-arene complexes were elucidated by various techniques. This is the first report that at least two reactions occur simultaneously during the photoreaction of an Os(II) arene complex, including the selective photodissociation of the biphenyl arene ligand and oxidation of Os(II) to Os(III) induced by irradiation with blue light or UVA. The released biphenyl ligand, the translocation of the Os-arene or arene-depleted species from mitochondria to the nucleus, might be responsible for the DNA damage and inhibition of colony formation, as well as contribute to overcoming cisplatin resistance. Furthermore, mitochondrial damage, apoptosis, and ROS generation might arise from oxidation of Os(II) to Os(III) in the photoreaction. The present studies have investigated the photocytotoxicity, anticancer mechanism of action, and photochemical decomposition pathways for Os(II)-arene complexes. **OsCUR-2** particularly appears to be a candidate for further development as a phototherapeutic agent with the potential to overcome cisplatin resistance. This work provides a new strategy to generate novel anticancer drugs via release of arene ligands and oxidation of metal centers upon light irradiation.

EXPERIMENTAL SECTION

Materials and Synthesis. The ligand curcumin was purchased from HEOWNS. The starting metal-arene dimeric materials ($[(\eta^6$-*p*-cymene)$OsCl_2]_2$, $[(\eta^6$-biphenyl)$OsCl_2]_2$, $[(\eta^6$-biphenyl)$OsI_2]_2$, and $[(\eta^6$-biphenyl)$RuCl_2]_2$) were prepared according to previously reported procedures.[39] All other chemicals and reagents were commercially available and were used as-received. MTDR was purchased from Invitrogen, and DCFH-DA was purchased from Sigma-Aldrich. Antibodies were purchased as follows: anticaspase-3 (SC-7148; Santa Cruz Biotechnology, Inc.), anti-GAPDH (AP0063; Abgent, Suzhou, China), anti-γ-H2AX (ab2893; Abcam, Cambridge, MA, USA), and antivinculin antibody (MAB3574, Millipore).

[Os(*p*-cymene)(Curc)Cl] (OsCUR-1). This compound was obtained by a two-step reaction. The curcumin was dissolved in methanol, and NaOMe was added. After 1 h stirring at room temperature, $[(\eta^6$-*p*-cymene)$OsCl_2]_2$ was added. The resulting dark-red solution was stirred and refluxed for 24 h. The solvent was removed under reduced pressure, and the residual was redissolved in dichloromethane. Sodium chloride was filtered from the mixture. An orange-red precipitate was obtained after rotary evaporation, and this precipitate was purified by TLC with dichloromethane/methanol as the eluent; further purification was performed by recrystallization from $CHCl_3$. Reaction yield 68%. ^{1}H NMR (400 MHz, DMSO-d_6) δ 9.56 (s, 2H), 7.41 (d, 2H), 7.24 (d, 2H), 7.06 (d, 2H), 6.81 (d, 2H), 6.56 (d, 2H), 6.14 (d, 2H), 5.91 (d, 2H), 5.68 (s, 1H), 3.83 (s, 6H), 2.80−2.59 (m, 1H), 2.22 (s, 3H), 1.28 (d, 6H). ESI-MS (in CH_3CN): calcd for $[(\eta^6$-*p*-cym)Os(curcuminato)$]^+$ m/z 691.82, found m/z 693.42. Anal. Calcd for **OsCUR-1** ($C_{31}H_{33}O_6ClOs$, %): C, 51.20; H, 4.57. Found (%): C, 50.88; H, 4.58.

[Os(biphenyl)(Curc)Cl] (OsCUR-2). This compound was synthesized by using a procedure similar to **OsCUR-1** except replacing $[(\eta^6$-*p*-cymene)$OsCl_2]_2$ with $[(\eta^6$-biphenyl)$OsCl_2]_2$. Reaction yield 73%. ^{1}H NMR (400 MHz, DMSO-d_6) δ 9.54 (s, 2H), 7.78 (d, 3.1 Hz, 2H), 7.49 (m, 3H), 7.15 (t, 4H), 7.00 (d, 2H), 6.80 (d, 2H), 6.66 (d, 2H), 6.48 (d, 2H), 6.40 (t, 2H), 6.30 (t, 1H), 5.63 (s, 1H), 3.83 (s, 6H). ESI-MS (in CH_3CN): calcd for $[(\eta^6$-biphenyl)Os(curcuminato)$]^+$ m/z 711.81, found m/z 713.33. Anal. Calcd for **OsCUR-2** ($C_{33}H_{29}O_6ClOs$, %): C, 53.04; H, 3.91. Found (%): C, 52.16; H, 4.21.

[Ru(biphenyl)(Curc)Cl] (RuCUR-2). A similar method was adopted for the synthesis of **RuCUR-2** as for **OsCUR-1** in which precursor $[(\eta^6$-p-cymene)$OsCl_2]_2$ was replaced by $[(\eta^6$-biphenyl)$RuCl_2]_2$. Reaction yield 80%. ^{1}H NMR (500 MHz, $CDCl_3$) δ 7.81 (d, 2H), 7.50 (m, 3H), 7.04−6.92 (m, 4H), 6.89 (d, 2H), 6.35 (d, 2H), 5.98 (t, 2H), 5.87 (d, 2H), 5.80 (d, 3H), 5.41 (s, 1H), 3.94 (s, 6H). ESI-MS (in CH_3CN): calcd for $[(\eta^6$-biphenyl)Ru(curcuminato)$]^+$ m/z 622.25, found m/z 623.25. Anal. Calcd for **RuCUR-2** ($C_{33}H_{29}O_6ClRu(H_2O)_{0.66}(CH_2Cl_2)_{0.66}$, %): C, 55.64; H, 4.39. Found (%): C, 55.87; H, 4.73.

[Os(biphenyl)(dpq)I]PF$_6$ (OsDPQ-2). $[(\eta^6$-biphenyl)$OsI_2]_2$ was mixed with dpq and dissolved in ethanol. The solution was stirred under reflux at 353 K for 2 h. The solution color changed from brown to orange. The solution was hot-filtered, and ammonium hexafluorophosphate (68.1 mg, 0.418 mmol) was added. The yellow-orange precipitate was collected by vacuum filtration and washed with ethanol and diethyl ether. It was dried under vacuum overnight. Yield: 47.1 mg (65.9%). ESI-MS calcd for $C_{26}H_{18}IN_4Os$ m/z 705.2, found m/z 704.9. ^{1}H NMR (600 MHz, acetone-d_6) δ 9.74 (d, 2H, J = 6 Hz), 9.67 (d, 2H, J = 6 Hz), 9.38 (s, 2H), 8.15 (dd, 2H, J = 6 Hz), 7.55 (d, 2H, J = 6 Hz), 7.45 (t, 1H, J = 6 Hz), 7.33 (t, 2H, J = 6 Hz), 7.02 (d, 2H, J = 6 Hz), 6.92 (t, 2H, J = 6 Hz), 6.71 (t, 1H, J = 6 Hz). Anal.

https://doi.org/10.1021/acs.inorgchem.1c00241
Inorg. Chem. 2021, 60, 17450−17461

Calcd for **OsDPQ-2** ($C_{26}H_{18}F_6IN_4OsP$, %): C, 36.80 H, 2.14, N, 6.60. Found (%): C, 36.55; H, 2.11; N, 6.39.

[Os(biphenyl)(bpy)I]PF$_6$ (OsBPY-2). [(η^6-biphenyl)OsI_2]$_2$ was mixed with bpy and dissolved in ethanol. The solution was stirred under reflux at 353 K for 2 h. There solution color changed from dark brown to orange. The solution was hot-filtered, and ammonium hexafluorophosphate (137.6 mg, 0.844 mmol) was added. The orange precipitate was collected by vacuum filtration and washed with ethanol and diethyl ether. It was dried under vacuum overnight. Yield: 104.9 mg (80.5%). ESI-MS calcd for $C_{22}H_{18}IN_2Os$: m/z 629.0, found m/z 629.0. ^{1}H NMR (600 MHz, acetone-d$_6$) δ 9.21 (d, 2H, J = 6.0 Hz), 8.65 (d, 2H, J = 6.0 Hz), 8.14 (t, 2H, J = 6.0 Hz), 7.53 (t, 2H, J = 6.0 Hz), 7.48 (d, 2H, J = 6.0 Hz), 7.40 (d, 1H, J = 6.0 Hz), 7.33 (t, 2H, J = 6.0 Hz), 6.86 (d, 2H, J = 6.0 Hz), 6.56 (t, 2H, J = 6.0 Hz), 6.50 (t, 1H, J = 6.0 Hz). Anal. Calcd for **OsBPY-2** ($C_{22}H_{18}F_6IN_2OsP$, %): C, 34.21; H, 2.35; N, 3.63. Found (%): C, 34.45; H, 2.29; N, 3.61.

ASSOCIATED CONTENT

Supporting Information

The Supporting Information is available free of charge at https://pubs.acs.org/doi/10.1021/acs.inorgchem.1c00241.

> Characterization of complexes **OsCUR-1**, **OsCUR-2**, **RuCUR-2**, **OsDPQ-2**, and **OsBPY-2** including ^{1}H NMR spectra, ESI-MS, elemental analyses, single-crystal X-ray structure analysis, and UV−vis and fluorescence spectroscopic properties; computational details; biological procedures such as ICP-MS measurement, MTT detection, confocal microscopy imaging, and Western blotting experiments (PDF)

Accession Codes

CCDC 1571503 contains the supplementary crystallographic data for this paper. These data can be obtained free of charge via www.ccdc.cam.ac.uk/data_request/cif, or by emailing data_request@ccdc.cam.ac.uk, or by contacting The Cambridge Crystallographic Data Centre, 12 Union Road, Cambridge CB2 1EZ, UK; fax: +44 1223 336033.

AUTHOR INFORMATION

Corresponding Authors

Zhi Su − *Jiangsu Collaborative Innovation Center of Biomedical Functional Materials, School of Chemistry and Materials Science, Nanjing Normal University, Nanjing 210023, China*; orcid.org/0000-0003-1690-527X; Email: zhisu@njnu.edu.cn

Martin J. Paterson − *Institute of Chemical Sciences, School of Engineering & Physical Sciences, Heriot-Watt University, Edinburgh, Scotland EH14 4AS, U.K.*; orcid.org/0000-0002-0012-974X; Email: M.J.Paterson@hw.ac.uk

Zong-Wan Mao − *MOE Key Laboratory of Bioinorganic and Synthetic Chemistry, School of Chemistry, Sun Yat-Sen University, Guangzhou 510275, China*; orcid.org/0000-0001-7131-1154; Email: cesmzw@mail.sysu.edu.cn

Hong-Ke Liu − *Jiangsu Collaborative Innovation Center of Biomedical Functional Materials, School of Chemistry and Materials Science, Nanjing Normal University, Nanjing 210023, China*; orcid.org/0000-0002-0968-6518; Email: liuhongke@njnu.edu.cn

Peter J. Sadler − *Department of Chemistry, University of Warwick, Coventry CV4 7AL, U.K.*; orcid.org/0000-0001-9160-1941; Email: P.J.Sadler@warwick.ac.uk

Authors

Xuling Xue − *Jiangsu Collaborative Innovation Center of Biomedical Functional Materials, School of Chemistry and Materials Science, Nanjing Normal University, Nanjing 210023, China*

Ying Fu − *Department of Chemistry, University of Warwick, Coventry CV4 7AL, U.K.; National Center for Advancing Translational Sciences (NCATS/NIH), Rockville, Maryland 20850, United States*

Liang He − *MOE Key Laboratory of Bioinorganic and Synthetic Chemistry, School of Chemistry, Sun Yat-Sen University, Guangzhou 510275, China*

Luca Salassa − *Donostia International Physics Center, Donostia 20018, Spain; Ikerbasque, Basque Foundation for Science, Bilbao 48011, Spain; Kimika Fakultatea, Euskal Herriko Unibertsitatea, UPV/EHU, Donostia 20080, Spain*

Ling-Feng He − *Jiangsu Key Laboratory for Molecular and Medical Biotechnology, College of Life Science, Nanjing Normal University, Nanjing 210023, China*

Yuan-Yuan Hao − *Jiangsu Collaborative Innovation Center of Biomedical Functional Materials, School of Chemistry and Materials Science, Nanjing Normal University, Nanjing 210023, China*

Madeleine J. Koh − *Department of Chemistry, University of Warwick, Coventry CV4 7AL, U.K.*

Clément Soulié − *Institute of Chemical Sciences, School of Engineering & Physical Sciences, Heriot-Watt University, Edinburgh, Scotland EH14 4AS, U.K.*

Russell J. Needham − *Department of Chemistry, University of Warwick, Coventry CV4 7AL, U.K.*

Abraha Habtemariam − *Department of Chemistry, University of Warwick, Coventry CV4 7AL, U.K.*

Claudio Garino − *Department of Chemistry and NIS Interdepartmental Center, University of Turin, Turin I-10135, Italy*; orcid.org/0000-0002-7854-6076

Kirill A. Lomachenko − *Department of Chemistry and NIS Interdepartmental Center, University of Turin, Turin I-10135, Italy; European Synchrotron Radiation Facility, 38043 Grenoble, France; The Smart Materials Research Institute, Southern Federal University, Rostov-on-Don 344090, Russia*; orcid.org/0000-0003-0238-1719

Yong Qian − *Jiangsu Collaborative Innovation Center of Biomedical Functional Materials, School of Chemistry and Materials Science, Nanjing Normal University, Nanjing 210023, China*

Complete contact information is available at: https://pubs.acs.org/10.1021/acs.inorgchem.1c00241

Author Contributions

X.X., Y.F., L.H., L.S., and L.-F.H. contributed to this manuscript equally. X.X., Y.F., L.H., L.S., L.-F.H., Y.-Y.H., M.J.K., C.S., R.J.N., A.H., C.G., and K.A.L. designed and performed the experiments. Z.S., M.J.P., Z.-W.M., H.-K.L., and P.J.S. proposed and supervised the project. All the authors were involved in discussing the results and writing the manuscript.

Notes

The authors declare no competing financial interest.

ACKNOWLEDGMENTS

We thank Dr. Zhe Liu, Dr. Yao Zhao, and Dr. Lihong Li for their help with NMR and MS experiments and Dr. P. Glatzel,

Dr. E. Gallo, Dr. D. Gianolio, and Prof. C. Lamberti for the assistance during the XAS experiment at ID26 beamline of the ESRF. We thank NSFC (nos. 22077066, 21771109, 21778033, 21701195, 21837006, and 21977052), NSF of Jiangsu Province (no. BK20171472), ERC (grant 247450), EPSRC (grants EP/F034210/1, EP/P030572/1, EP/P001459, and EP/T021675), Anglo American Platinum, and the Severo Ochoa Centres of Excellence Programme for L.S. by the Spanish State Research Agency (ref CEX2018-000867-S) for their financial support.

■ REFERENCES

(1) Shi, H. Y.; Sadler, P. J. How promising is phototherapy for cancer? *Br. J. Cancer* **2020**, *123* (6), 871−873.

(2) Boros, E.; Dyson, P. J.; Gasser, G. Classification of metal-based drugs according to their mechanisms of action. *Chem.* **2020**, *6* (1), 41−60.

(3) Huang, H. Y.; Banerjee, S.; Qiu, K. Q.; Zhang, P. Y.; Blacque, O.; Malcomson, T.; Paterson, M. J.; Clarkson, G. J.; Staniforth, M.; Stavros, V. G.; Gasser, G.; Chao, H.; Sadler, P. J. Targeted photoredox catalysis in cancer cells. *Nat. Chem.* **2019**, *11* (11), 1041−1048.

(4) Liu, H. K.; Sadler, P. J. Metal complexes as DNA intercalators. *Acc. Chem. Res.* **2011**, *44* (5), 349−359.

(5) Xue, X. L.; Qian, C. G.; Tao, Q.; Dai, Y. X.; Lv, M. D.; Dong, J. W.; Su, Z.; Qian, Y.; Zhao, J.; Liu, H. K.; Guo, Z. J. Using bioorthogonally catalyzed lethality strategy to generate mitochondria-targeting antitumor metallodrugs *in vitro* and *in vivo*. *Natl. Sci. Rev.* **2020**, DOI: 10.1093/nsr/nwaa286.

(6) (a) Holder, A. A.; Zigler, D. F.; Tarrago-Trani, M. T.; Storrie, B.; Brewer, K. J. Photobiological impact of $[\{(bpy)_2Ru(dpp)\}_2RhCl_2]Cl_5$ and $[\{(bpy)_2Os(dpp)\}_2RhCl_2]Cl_5$ [bpy = 2,2′-bipyridine; dpp = 2,3-bis(2-pyridyl)pyrazine] on Vero cells. *Inorg. Chem.* **2007**, *46* (12), 4760−4762. (b) Smith, N. A.; Sadler, P. J. Photoactivatable metal complexes: from theory to applications in biotechnology and medicine. *Philos. Trans. R. Soc., A* **2013**, *371* (1995), 20120519. (c) Schatzschneider, U. Photoactivated biological activity of transition-metal complexes. *Eur. J. Inorg. Chem.* **2010**, *2010*, 1451−1467. (d) Imberti, C.; Zhang, P. Y.; Huang, H. Y.; Sadler, P. J. New designs for phototherapeutic transition metal complexes. *Angew. Chem., Int. Ed.* **2020**, *59*, 61−73.

(7) Wang, R.; Eberspacher, T. A.; Hasegawa, T.; Day, V.; Ware, D. C.; Taube, H. Tmtacn, tacn, and triammine complexes of (eta 6-arene) Os^{II}: syntheses, characterizations, and photosubstitution reactions (tmtacn = 1,4,7-trimethyl-1,4,7-triazacyclononane; tacn = 1,4,7-triazacyclononane). *Inorg. Chem.* **2001**, *40* (4), 593−600.

(8) Farrer, N. J.; Salassa, L.; Sadler, P. J. Photoactivated chemotherapy (PACT): the potential of excited-state d-block metals in medicine. *Dalton Trans.* **2009**, *48*, 10690−16701.

(9) Zhang, P. Y.; Huang, H. Y. Future potential of osmium complexes as anticancer drug candidates, photosensitizers and organelle-targeted probes. *Dalton Trans.* **2018**, *47* (42), 14841−14854.

(10) Needham, R. J.; Sanchez-Cano, C.; Zhang, X.; Romero-Canelon, I.; Habtemariam, A.; Cooper, M. S.; Meszaros, L.; Clarkson, G. J.; Blower, P. J.; Sadler, P. J. In-cell activation of organo-Osmium(II) anticancer complexes. *Angew. Chem., Int. Ed.* **2017**, *56* (4), 1017−1020.

(11) Peacock, A. F. A.; Parsons, S.; Sadler, P. J. Tuning the hydrolytic aqueous chemistry of osmium arene complexes with N,O-chelating ligands to achieve cancer cell cytotoxicity. *J. Am. Chem. Soc.* **2007**, *129* (11), 3348−3357.

(12) Coverdale, J. P. C.; Romero-Canelon, I.; Sanchez-Cano, C.; Clarkson, G. J.; Habtemariam, A.; Wills, M.; Sadler, P. J. Asymmetric transfer hydrogenation by synthetic catalysts in cancer cells. *Nat. Chem.* **2018**, *10* (3), 347−354.

(13) Pettinari, R.; Marchetti, F.; Pettinari, C.; Condello, F.; Petrini, A.; Scopelliti, R.; Riedel, T.; Dyson, P. J. Organometallic rhodium(III) and iridium(III) cyclopentadienyl complexes with curcumin and bisdemethoxycurcumin co-ligands. *Dalton Trans.* **2015**, *44* (47), 20523−20531.

(14) Pettinari, R.; Condello, F.; Marchetti, F.; Pettinari, C.; Smolenski, P.; Riedel, T.; Scopelliti, R.; Dyson, P. J. Dicationic ruthenium(II)-arene-curcumin complexes containing methylated 1,3,5-triaza-7-phosphaadamantane:synthesis, structure, and cytotoxicity. *Eur. J. Inorg. Chem.* **2017**, *2017* (22), 2905−2910.

(15) Caruso, F.; Rossi, M.; Benson, A.; Opazo, C.; Freedman, D.; Monti, E.; Gariboldi, M. B.; Shaulky, J.; Marchetti, F.; Pettinari, R.; Pettinari, C. Ruthenium-arene complexes of curcumin: X-ray and density functional theory structure, synthesis, and spectroscopic characterization, in vitro antitumor activity, and DNA docking studies of (p-cymene)Ru(curcuminato)chloro. *J. Med. Chem.* **2012**, *55* (3), 1072−1081.

(16) Pettinari, R.; Marchetti, F.; Condello, F.; Pettinari, C.; Lupidi, G.; Scopelliti, R.; Mukhopadhyay, S.; Riedel, T.; Dyson, P. J. Ruthenium(II)-arene RAPTA type complexes containing curcumin and bisdemethoxycurcumin display potent and selective anticancer activity. *Organometallics* **2014**, *33* (14), 3709−3715.

(17) Pettinari, R.; Marchetti, F.; Nicola, C. D.; Pettinari, C.; Cuccioloni, M.; Bonfili, L.; Eleuteri, A. M.; Therrien, B.; Batchelore, L. K.; Dyson, P. J. Novel osmium(II)-cymene complexes containing curcumin and bisdemethoxycurcumin ligands. *Inorg. Chem. Front.* **2019**, *6* (9), 2448−2457.

(18) Wilson, C. S.; Prior, T. J.; Sandland, J.; Savoie, H.; Boyle, R. W.; Murray, B. S. Homo- and hetero-dinuclear arene-linked osmium(II) and ruthenium(II) organometallics: probing the impact of metal variation on reactivity and biological activity. *Chem. - Eur. J.* **2020**, *26* (50), 11593−11603.

(19) Banerjee, S.; Chakravarty, A. R. Metal complexes of curcumin for cellular imaging, targeting, and photoinduced anticancer activity. *Acc. Chem. Res.* **2015**, *48* (7), 2075−2083.

(20) Wanninger, S.; Lorenz, V.; Subhan, A.; Edelmann, F. T. Metal complexes of curcumin-synthetic strategies, structures and medicinal applications. *Chem. Soc. Rev.* **2015**, *44* (15), 4986−5002.

(21) Bhattacharyya, U.; Kumar, B.; Garai, A.; Bhattacharyya, A.; Kumar, A.; Banerjee, S.; Kondaiah, P.; Chakravarty, A. R. Curcumin “drug” stabilized in oxidovanadium(iv)-bodipy conjugates for mitochondria-targeted photocytotoxicity. *Inorg. Chem.* **2017**, *56* (20), 12457−12468.

(22) Mitra, K.; Gautam, S.; Kondaiah, P.; Chakravarty, A. R. The cis-diammineplatinum(ii) complex of curcumin: a dual action dna crosslinking and photochemotherapeutic agent. *Angew. Chem.* **2015**, *127* (47), 14195−14199.

(23) Pucci, D.; Crispini, A.; Mendiguchia, B. S.; Pirillo, S.; Ghedini, M.; Morelli, S.; De Bartolo, L. Improving the bioactivity of Zn(II)-curcumin based complexes. *Dalton Trans.* **2013**, *42* (26), 9679−9687.

(24) Singh, J.; Alayon, E. M. C.; Tromp, M.; Safonova, O. V.; Glatzel, P.; Nachtegaal, M.; Frahm, R.; van Bokhoven, J. A. Generating highly active partially oxidized platinum during oxidation of carbon monoxide over Pt/Al_2O_3: in situ, time-resolved, and high-energy-resolution x-ray absorption spectroscopy. *Angew. Chem., Int. Ed.* **2008**, *47* (48), 9260−9264.

(25) Rosenberg, R. A.; Simons, J. K.; Frigo, S. P.; Tan, K.; Chen, J. M. X-ray fluorescence detection of low-Z elements using a microchannel plate detector. *Rev. Sci. Instrum.* **1992**, *63* (4), 2193−2194.

(26) Taylor, R. C.; Cullen, S. P.; Martin, S. J. Apoptosis: controlled demolition at the cellular level. *Nat. Rev. Mol. Cell Biol.* **2008**, *9* (3), 231−241.

(27) He, L.; Tan, C. P.; Ye, R. R.; Zhao, Y. Z.; Liu, Y. H.; Zhao, Q.; Ji, L. N.; Mao, Z. W. Theranostic iridium(III) complexes as one- and two- photon phosphorescent trackers to monitor autophagic lysosomes. *Angew. Chem., Int. Ed.* **2014**, *53* (45), 12137−12141.

(28) Prasad, P.; Pant, I.; Khan, I.; Kondaiah, P.; Chakravarty, A. R. Mitochondria-targeted photoinduced anticancer activity of oxidovanadium(IV) complexes of curcumin in visible light. *Eur. J. Inorg. Chem.* **2014**, *2014* (14), 2420−2431.

(29) Li, J.; Yuan, J. Caspases in apoptosis and beyond. *Oncogene* **2008**, *27* (48), 6194−6206.
(30) Li, Y. C.; Gu, Z. Y.; Zhang, C.; Li, S. H.; Zhang, L.; Zhou, G. Q.; Wang, S. X.; Zhang, J. C. Synthesis, characterization and ROS-mediated antitumor effects of palladium(II) complexes of curcuminoids. *Eur. J. Med. Chem.* **2018**, *144*, 662−671.
(31) LeBel, C. P.; Ischiropoulos, H.; Bondy, S. C. Evaluation of the probe 2′,7′-dichloroflurescin as an indicator of reactive oxygen species formation and oxidative stress. *Chem. Res. Toxicol.* **1992**, *5* (2), 227−231.
(32) Xue, X. L.; Qian, C. G.; Fang, H. B.; Liu, H. K.; Yuan, H.; Guo, Z. J.; Bai, Y.; He, W. J. Photoactivated lysosomal escape of a monofunctional Pt^{II} complex Pt-BDPA for nucleus access. *Angew. Chem., Int. Ed.* **2019**, *58* (36), 12661−12666.
(33) Zhang, L.; Cheng, X.; Gao, Y. Y.; Bao, J. D.; Guan, H. X.; Lu, R. R.; Yu, H. X.; Xu, Q.; Sun, Y. Induction of ROS-independent DNA damage by curcumin leads to G_2/M cell cycle arrest and apoptosis in human papillary thyroid carcinoma BCPAP cells. *Food Funct.* **2016**, *7* (1), 315−325.
(34) Friedl, P.; Alexander, S. Cancer invasion and the microenvironment: plasticity and reciprocity. *Cell* **2011**, *147* (5), 992−1009.
(35) Bordiga, S.; Groppo, E.; Agostini, G.; van Bokhoven, J. A.; Lamberti, C. Reactivity of surface species in heterogeneous catalysts probed by in situ X-ray absorption techniques. *Chem. Rev.* **2013**, *113* (3), 1736−1850.
(36) Lomachenko, K. A.; Garino, C.; Gallo, E.; Gianolio, D.; Gobetto, R.; Glatzel, P.; Smolentsev, N.; Smolentsev, G.; Soldatov, A. V.; Lamberti, C.; Salassa, L. High energy resolution core-level X-ray spectroscopy for electronic and structural characterization of osmium compounds. *Phys. Chem. Chem. Phys.* **2013**, *15* (38), 16152−16519.
(37) Garai, A.; Pant, I.; Banerjee, S.; Banik, B.; Kondaiah, P.; Chakravarty, A. R. Photorelease and cellular delivery of mitocurcumin from its cytotoxic cobalt(III) complex in visible light. *Inorg. Chem.* **2016**, *55* (12), 6027−6035.
(38) Garipler, G.; Mutlu, N.; Lack, N. A.; Dunn, C. D. Deletion of conserved protein phosphatases reverses defects associated with mitochondrial DNA damage in Saccharomyces cerevisiae. *Proc. Natl. Acad. Sci. U. S. A.* **2014**, *111* (4), 1473−1478.
(39) Peacock, A. F. A.; Habtemariam, A.; Fernandez, R.; Walland, V.; Fabbiani, F. P. A.; Parsons, S.; Aird, R. E.; Jodrell, D. I.; Sadler, P. J. Tuning the reactivity of osmium(II) and ruthenium(II) arene complexes under physiological conditions. *J. Am. Chem. Soc.* **2006**, *128* (5), 1739−1748.
(40) Becke, A. D. Density-functional thermochemistry. III. The role of exact exchange. *J. Chem. Phys.* **1993**, *98* (7), 5648−5652.
(41) Hay, P. J.; Wadt, W. R. Ab initio Effective core potentials for molecular calculations-Potentials for the transition-metal atoms Sc to Hg. *J. Chem. Phys.* **1985**, *82* (1), 270−283.
(42) McLean, A. D.; Chandler, G. S. Contracted Gaussian basis sets for molecular calculations. I. Second row atoms, Z = 11−18. *J. Chem. Phys.* **1980**, *72* (10), 5639−5648.
(43) (a) Vĺcek, A., Jr.; Źalis, S. Modeling of charge-transfer transitions and excited states in d^6 transition metal complexes by DFT techniques. *Coord. Chem. Rev.* **2007**, *251* (3−4), 258−287. (b) Casida, M. E.; Jamorski, C.; Casida, K. C.; Salahub, D. R. Molecular excitation energies to high-lying bound states from time dependent density-functional response theory: Characterization and correction of the time-dependent local density approximation ionization threshold. *J. Chem. Phys.* **1998**, *108* (11), 4439−4449.
(44) Krauklis, V. I.; Reshetova, I. K.; Podkopaeva, Y. O.; Chizhov, V. Y. Electronically exited states in triphenylphosphine complexes of Ruthenium (II): TD DFT study. *J. Photochem. Photobiol., A* **2018**, *354*, 112−118.
(45) Browne, W. R.; O'Boyle, N. M.; McGarvey, J. J.; Vos, J. G. Elucidating excited state electronic structure and intercomponent interactions in multicomponent and supramolecular systems. *Chem. Soc. Rev.* **2005**, *34* (8), 641−663.
(46) Ramírez-Solís, A.; Daudey, J. P. Ab initio study on the spectroscopy of $CuCl_2$. II. Benchmark calculations on the X_2Pi g-C_2Deltag and X_2Pi g-D_2Deltag transitions. *J. Chem. Phys.* **2005**, *122* (1), 014315.
(47) Das, D.; Scherer, T. M.; Das, A.; Mondal, T. K.; Mobin, S. M.; Fiedler, J.; Priego, J. L.; Jiménez-Aparicio, R.; Kaim, W.; Lahiri, G. K. The intricate paramagnetic state of $[Os(Q)_2(bpy)]^+$, Q = 4,6-di-tert-butyl-o- iminobenzoquinone. *Dalton Trans.* **2012**, *41* (38), 11675−11683.